

Magnetostructural Effect in the Multiferroic BiFeO₃-BiMnO₃ Checkerboard from First Principles

L. Pálová, P. Chandra and K. M. Rabe

Department of Physics and Astronomy, Rutgers University, Piscataway, NJ 08854

(Dated: June 10, 2021)

Using first principles calculations, we present a magnetostructural effect in the BiFeO₃-BiMnO₃ nanocheckerboard that is not found in either bulk parent compound or in BiFeO₃-BiMnO₃ superlattices. We also demonstrate that the atomic-scale checkerboard has a multiferroic ground state with the desired properties of each constituent material: polar and ferrimagnetic due to BiFeO₃ and BiMnO₃ respectively.

PACS numbers: 75.80.+q, 77.80.-e, 75.75.+a

There is currently tremendous interest in finding new multiferroic (ferroelectric and ferromagnetic) materials with large magnetoelectric coupling. Advances in the synthesis of artificially structured materials have stimulated efforts to design new multiferroic heterostructures, with first principles methods being an essential tool for the identification and investigation of promising systems. In this Letter, we report the first-principles identification and characterization of an unusual heterostructure, a multiferroic atomic-scale 2D nanocheckerboard^{1,2,3,4} of BiFeO₃-BiMnO₃, with properties that critically depend on the geometry and are not present in either bulk or layered structures of the constituent materials. In particular, the 2D checkerboard geometry leads to magnetic frustration and to quasi-degenerate magnetic states that can be tuned by an external perturbation that changes the crystal structure, such as an electric field. This results in a novel magnetostructural effect, adding to previous examples of magnetostructural coupling such as bulk⁵ and layered⁶ manganites, epitaxial *EuTiO*₃⁷ and *EuSe/PbSe*_{1-x}*Te*_x multilayers.⁸

Our first principles calculations are performed using density functional theory within the local spin-density approximation (LSDA)+U method as implemented in the Vienna Ab-initio Simulation Package VASP-4.6.34⁹. We test the robustness of our results with two different implementations of the rotationally invariant LSDA+U version, the first as introduced by Liechtenstein¹⁰ with $U_{Fe} = U_{Mn} = 5eV$, $J_{Fe} = J_{Mn} = 1eV$, and the second due to Dudarev¹¹, with $U_{Mn}^{eff} = 5.2eV$, $U_{Fe}^{eff} = 4eV$, where $U^{eff} = U - J$. It has been shown that these U and J values match experimental data in bulk BiFeO₃¹²; the value $U^{eff} = 5.2eV$ has been used for previous bulk BiMnO₃ ground state calculations¹³. We use projector-augmented wave potentials (PAW)^{14,15} and treat explicitly 15 valence electrons for Bi ($5d^{10}6s^26p^3$), 14 for Fe ($3p^63d^64s^2$), 13 for Mn ($3p^63d^54s^2$), and 6 for O ($2s^22p^4$). The cutoff energies for the plane wave basis set are 550eV and 800eV in the ionic relaxations and for subsequent self-consistent energy calculations respectively. Gaussian broadening of the partial occupancies for each wavefunction is 0.05eV. A Monkhorst-Pack k-point grid¹⁶ is generated with density $4 \times 4 \times 4$ for

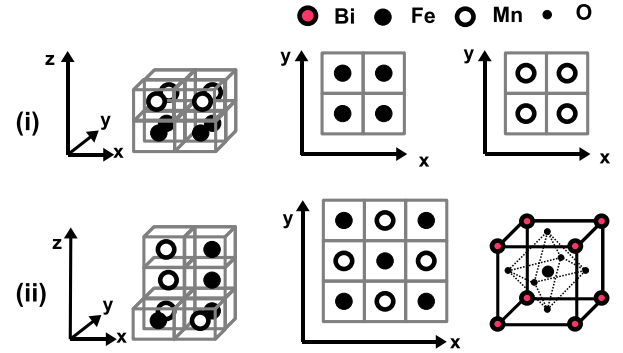


Figure 1: (i) BiFeO₃-BiMnO₃ superlattice with alternation of Fe/Mn planes. (ii) (left) BiFeO₃-BiMnO₃ checkerboard. Checkerboard ordering of Fe/Mn atoms in the (xy) plane, pillars of the same composition form along the z -direction. (right) Ideal perovskite unit cell. Perovskite cells with Fe/Mn atoms on the B-site repeat according to the checkerboard pattern (ii), or layered geometry (i).

$(\sqrt{2} \times \sqrt{2} \times 1)a_0$ double perovskite and $4 \times 4 \times 2$ for $(\sqrt{2} \times \sqrt{2} \times 2)a_0$ four perovskite cells. Ions are relaxed towards equilibrium positions until the Hellmann-Feynman forces are less than $10^{-3}eV/\text{\AA}$. The spontaneous polarization is calculated by the Berry phase method¹⁷ with k-point mesh twice as dense as in the energy calculations.

We consider four formula units (perovskite cells), two each with Fe and Mn atoms on the B-site, which we repeat periodically in space. For the planar checkerboard, we alternate iron (Fe) and manganese (Mn) atoms at the atomic level to form pillars of the same composition as in Fig. 1(ii). For the layered superlattice, we alternate single unit cell layers along z , as in Fig. 1(i). In both cases, the supercell is $\sqrt{2}a_0 \times \sqrt{2}a_0 \times 2a_0$.

We study various collinear spin orderings of the magnetic Fe and Mn atoms, shown for the checkerboard in Fig. 2. FeFM and FeAFM refer to ferromagnetic and antiferromagnetic ordering respectively for the Fe moments in the relevant structural component (pillar for the checkerboard, layer for the superlattice); similarly MnFM and MnAFM describe the spin ordering of the

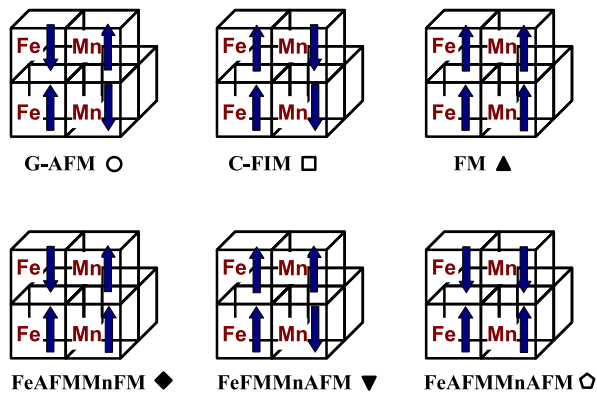


Figure 2: From top left to bottom right: (i) G-AFM: rocksalt type antiferromagnetic (AFM) order, (ii) C-FIM: AFM order in horizontal planes, ferromagnetic (FM) order along Fe/Mn pillars, (iii) FM order, (iv) FeAFMMnFM: AFM order along Fe pillars, FM order along Mn pillars, (v) FeFMMnAFM: FM order along Fe pillars, AFM order along Mn pillars, (vi) FeAFMMnAFM: AFM order along Fe/Mn pillars, but FM order in horizontal planes.

Mn moments. In the checkerboard, this notation fully specifies the states considered. For the superlattice, the remaining ambiguity is resolved as follows: FeAFMMnAFM magnetic order designates AFM ordered Fe and Mn planes with FM order along the mixed Fe-Mn chains in the z direction, while G-AFM designates the case with AFM order along the mixed chains; similarly, FeFMMnFM designates FM ordered Fe and Mn planes with AFM order along the mixed Fe-Mn chains in the z direction, while FM designates the case with FM order along the mixed chains.

In searching for the ground state crystal structure for each spin ordering, we consider structures generated by three typically unstable modes of the cubic perovskite structure:¹⁸ the zone center polar mode Γ_4^- , the M_3^+ oxygen octahedron rotations (all rotations about a given axis in phase) and R_4^+ rotations (sense of rotations alternates along the rotation axis). We freeze in selected modes and combinations of modes and optimize atomic displacements and lattice parameters in the resulting space groups.

First, to investigate the effect of B -site cation geometry on the magnetic ordering, we present results in Table I for the magnetic ordering energies when the structures are held fixed to the ideal perovskite reference structure. In the layered superlattice and both bulk parent systems, the difference in energy between magnetic ground state (FeAFMMnFM in the superlattice, G-AFM in bulk BiFeO₃ and FM in bulk BiMnO₃) and the first alternative state is $0.11 - 0.12 eV/f.u.$; this difference corresponds to a relatively large energy and we do not expect a transition to a different magnetic state. The highest energy magnetic states are more than $0.26 eV/f.u.$ apart. On the other hand in the checkerboard, all mag-

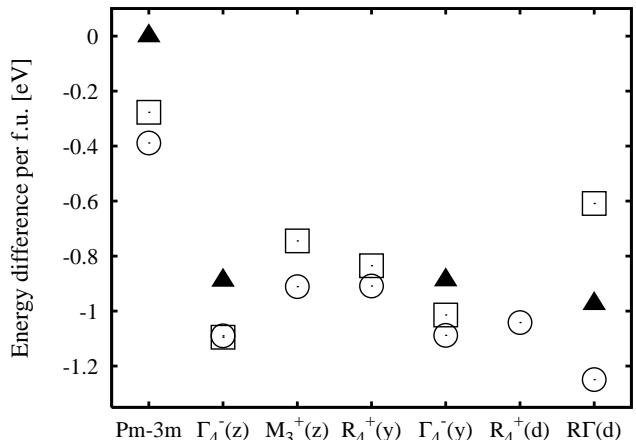


Figure 3: Structural energetics of bulk BiFeO₃. Energy difference per perovskite cell (f.u.) for different magnetic orderings (see Fig. 2) and structural distortions: (1) $Pm\bar{3}m$: no distortion - ideal perovskite, (2) $\Gamma_4^-(z)$: polar distortion along z axis, (3) $M_3^+(z)$: + oxygen octahedra tilts about z axis, (4) $R_4^+(y)$: - oxygen octahedra tilts about y axis, (5) $R_4^+(y)$ and $\Gamma_4^-(y)$ ($R\Gamma(y)$): linear combination of (4) and (2) along y axis, relaxes back to polar $\Gamma_4^-(y)$ with zero tilting angle, (6) $R_4^+([111])$ ($R_4^+(d)$): - oxygen octahedra tilts about $[111]$ axis, (7) $R_4^+([111])$ and $\Gamma_4^-([111])$ ($R\Gamma(d)$): linear combination of (6) and (2) along $[111]$ (d), where d refers to the cube diagonal direction.

netic states are found quasi-degenerate and are confined within the energetical window of $0.12 eV/f.u.$, that is, all are lower than the lowest states in the layered superlattice and bulk parent compounds. Indeed, the closest magnetic state to the FeAFMMnFM ground state is now only $0.022 eV/f.u.$ higher, making it much more plausible for a magnetic transition to occur.

Next we study the energetics of the structural distortion and its effect on the spin order. Before discussing results for the BiFeO₃-BiMnO₃ checkerboard, we look at the structural energetics of the two bulk constituent materials, BiFeO₃ and BiMnO₃. We plot energies for various magnetic orderings in seven types of structural distortions of bulk BiFeO₃ in Fig. 3. Our calculation verifies the R3c ground state of BiFeO₃: counter-rotations of the oxygen octahedra (R_4^+) and polar ionic distortions (Γ_4^-) along the $[111]$ axis are most energetically favorable.^{12,19} The ground state structure has G-type AFM order and spontaneous polarization $90 \mu C/cm^2$ along $[111]$ axis. For all structural distortions considered, the lowest energy magnetic ordering is G-AFM.

We study the structural energetics of bulk BiMnO₃ in a similar way; the plotted energies for various structural distortions and magnetic orderings are presented in Fig. 4. We find the lowest energy structure with R3c symmetry, the same as the ground state of BiFeO₃. The lowest energy structure has a half-metallic character and is

Table I: Calculated magnetic energies in an ideal perovskite setting with lattice constant $a_0 = 3.893\text{\AA}$ for various magnetic states in the checkerboard, layered superlattice, and bulk BiFeO_3 and BiMnO_3 . Value of $U = 5eV$ and $J = 1eV$ is used.

checkerboard		layered superlattice		BiFeO_3		BiMnO_3	
magnetic state	$\Delta E[eV/f.u.]$	magnetic state	$\Delta E[eV/f.u.]$	mag. state	$\Delta E[eV/f.u.]$	mag. state	$\Delta E[eV/f.u.]$
FeAFMMnFM	0.000	FeAFMMnFM	0.000	-	-	-	-
FM	0.022	FM	0.111	FM	0.360	FM	0.000
C-FIM	0.076	FeFMMnFM	0.136	C-AFM	0.115	C-AFM	0.293
FeAFMMnAFM	0.081	FeAFMMnAFM	0.135	A-AFM	0.223	A-AFM	0.116
G-AFM	0.114	G-AFM	0.181	G-AFM	0.000	G-AFM	0.494
FeFMMnAFM	0.119	FeFMMnAFM	0.260	-	-	-	-

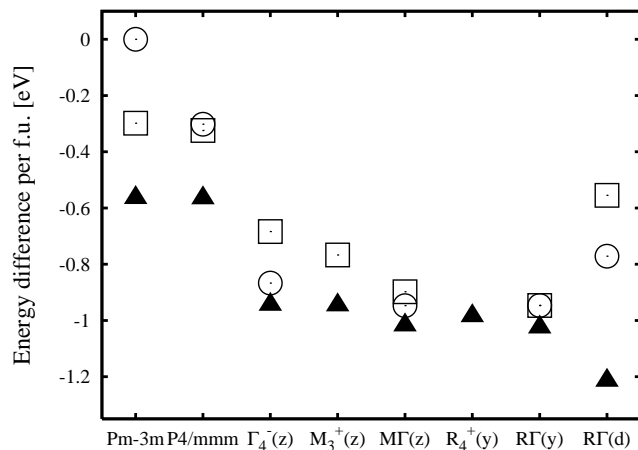


Figure 4: Structural energetics of bulk BiMnO_3 . Energy difference per perovskite cell (f.u.) for various structural distortions (see Fig. 3) and magnetic orderings (see Fig. 2); $P4/mmm$ corresponds to a tetragonally distorted perovskite cell with ideally positioned atoms and $M\Gamma(z)$ is a linear combination of rotational $M_3^+(z)$ and polar $\Gamma_4^-(z)$ modes.

ferromagnetic. This structure is not the monoclinic centrosymmetric ground state $C2/c$ of bulk BiMnO_3 which has a larger unit cell than that considered here.²⁰ However our calculation shows that it lies close to the ground state (only $43\text{ meV}/f.u.$ above the GS). For all structural distortions considered, the lowest energy magnetic ordering is FM.

In the layered BiFeO_3 - BiMnO_3 superlattice, we calculate magnetic energies for the rocksalt type G-AFM and FeAFMMnFM layered magnetic states in two structural distortions. For $R_4^+(y)$ & $\Gamma_4^-(y)$, we find $\Delta E = -0.504eV/f.u.$ for G-AFM and $\Delta E = -0.553eV/f.u.$ for FeAFMMnFM with respect to the FeAFMMnFM magnetic state in the ideal perovskite cell (see Table I). For $R_4^+([111])$ & $\Gamma_4^-([111])$, we find $\Delta E = -0.752eV/f.u.$ for G-AFM and $\Delta E = -0.761eV/f.u.$ for FeAFMMnFM. For both structural distortions considered, the lowest energy magnetic ordering is FeAFMMnFM.

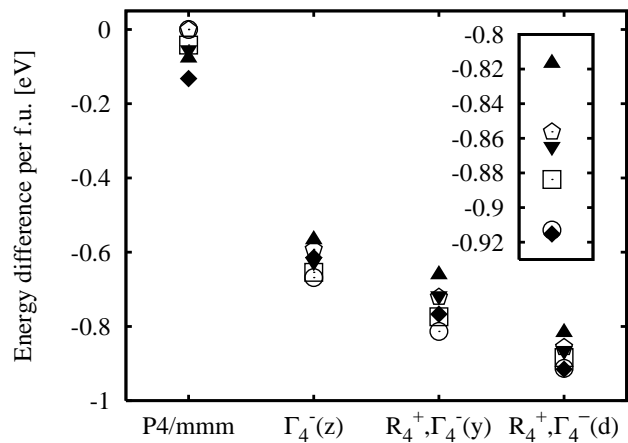


Figure 5: Structural energetics of BiFeO_3 - BiMnO_3 checkerboard. Energy difference per perovskite cell (f.u.) for different magnetic orderings (see Fig. 2) and structural distortions: (1) $P4/mmm$, (2) $\Gamma_4^-(z)$, (3) $R_4^+(y)$ and $\Gamma_4^-(y)$, (4) $R_4^+([111])$ and $\Gamma_4^-([111])$ ($R_4^+, \Gamma_4^-(d)$). Inset: zoomed view of the magnetic energies of c-R3c (4) distortion.

Let us now look at the results for the structural energetics of the BiFeO_3 - BiMnO_3 checkerboard. In Fig. 5, we present the energies for four different types of structural distortions. These types of distortions show the lowest energies among a larger set of structures that we explored.²¹ Notice that the variation of the structural energy is much larger than that of the magnetic energy of the checkerboard.

Not surprisingly, the $R_4^+([111])$ and $\Gamma_4^-([111])$ (R3c) type of structural distortion is energetically the most favorable; it is the BiFeO_3 ground state and the BiMnO_3 lowest energy structural distortion. The R3c symmetry is now broken due to pillar cation ordering and the space group of the checkerboard ground state becomes $P1$; we use the notation c-R3c, where c designates ‘‘checkerboard’’, as a reminder of the origin of the distortions. As shown in the inset of Fig. 5, the two lowest magnetic states G-AFM and FeAFMMnFM, are only $2\text{ meV}/f.u.$

apart. The ground state of the checkerboard has the FeAFMMnFM magnetic order, where Fe spins are ordered antiferromagnetically (AFM) along the Fe pillars, Mn spins are ordered ferromagnetically (FM) along the Mn pillars, reflecting “AFM” and “FM” nature of the parent BiFeO₃ and BiMnO₃ compounds respectively. A total magnetic moment $3.7\mu_B$ per Fe-Mn pair results from manganese chains. The FeAFMMnFM ground state is insulating with energy gap $0.88eV$, and we calculate a value of the polarization $62\mu C/cm^2$ pointing in the $[0.85, 0.85, 1]$ direction. The ground state of the checkerboard is multiferroic, being ferroelectric and ferrimagnetic.

In particular we want to relate and contrast the properties of the BiFeO₃-BiMnO₃ checkerboard to those of its two bulk constituent materials; we recall that BiFeO₃ is polar and antiferromagnetic, while BiMnO₃ is non-polar and ferromagnetic, and we have found that the checkerboard assumes the desired ferromagnetic-ferroelectric properties of each leading to a multiferroic ground-state whose magnetic behavior is structurally sensitive. We attribute this behavior to the development of a quasi-degenerate manifold of magnetic states in the checkerboard, in contrast to the gapped states in the layered superlattice and in the bulk; this can be understood in terms of frustration of the cations inherent in the checkerboard geometry. Since bulk BiFeO₃ is known to be G-AFM, and bulk BiMnO₃ FM, the Fe-Fe and Mn-Mn interactions tend to be AFM and FM-like respectively. In the layered superlattice, each Fe(Mn) atom has four Fe(Mn) and only two Mn(Fe) nearest neighbours, so that the Fe/Mn layers prefer to be AFM/FM, leading to minor frustration between the minority of mixed Fe-Mn bonds. The FeAFMMnFM layered ground state is much more preferable and lower in energy than any other magnetic state. In the checkerboard there are more frustrated bonds per each cation, and therefore more weight is given to the mixed Fe-Mn bonds and various magnetic states compete energetically.

We study the sensitivity of the closely spaced magnetic levels in the checkerboard to a structural distortion. As we tune the system from the checkerboard c-R3c ground state to c-I4cm state with $R_4^+(y)\&\Gamma_4^-(y)$ distortions, either the FeAFMMnFM (filled diamond) or the G-AFM (open circle) lowest state is favored. Switching between these two magnetic states occurs as we tune the system to other structural distortions (see Fig. 5). It is the competition between these two magnetic types that allows switching between nonzero and zero magnetization; the magnetostructural effect leads to the possibility of a structurally-driven magnetic transition in the checkerboard. This could be realized, for example, by imposing epitaxial strain constraints.

In summary, we present a magnetostructural effect in the atomic-scale checkerboard BiFeO₃-BiMnO₃, which is not present in either bulk or in layered structures of these two materials. Furthermore, unlike its parent compounds, the checkerboard has a multiferroic ground state with a nonzero magnetization and polarization; this is a new example of a nanocomposite with properties that can be designed. We note that this behavior is due to the magnetic frustration in this system inherent to the checkerboard geometry; as a result the magnetic states are quasi-degenerate and can be tuned by small perturbations including strain. We remark that our first principles calculations do not include spin-orbit coupling which is known to lead to weak ferromagnetism in bulk BiFeO₃.²² We expect that such corrections will not change our results fundamentally, but this is certainly worth pursuing in future work. We would also plan to investigate similar checkerboards on longer length-scales to make more direct contact with the possibility of future experiments.

We thank V. R. Cooper, M. Dawber, C.-J. Eklund, C. Fennie, A. Malashevich, M. Marsman and D. Vanderbilt for helpful discussions. This work was supported in part by NSF MRSEC DMR-0820404, NSF NIRT-ECS-0608842 and by the US Army Research Office through MURI-DAAD 19-01-1-0517.

-
- ¹ H. Zheng et al., *Science* **303**, 661 (2004).
² S. Yeo et al., *Appl. Phys. Lett.* **89**, 233120 (2006); C. L. Zhang et al., *Appl. Phys. Lett.* **90**, 133123 (2007); C. L. Zhang et al., *Appl. Phys. Lett.* **91**, 233110 (2007).
³ B. S. Gupton and P. K. Davies, *Nature Mater.* **6**, 586 (2007).
⁴ J. L. MacManus-Driscoll et al., *Nature Mater.* **7**, 314 (2008).
⁵ D. P. Kozlenko et al., *J. Magn. Mag. Mat.* **258-259**, 290 (2003).
⁶ T. Murata et al., *J. Magn. Mag. Mat.* **310**, 1555 (2007).
⁷ C. J. Fennie and K. M. Rabe, *Phys. Rev. Lett.* **97**, 267602 (2006).
⁸ R. T. Lechner et al., *Phys. Rev. Lett.* **94**, 157201 (2005).
⁹ G. Kresse and J. Hafner, *Phys. Rev. B* **47**, R558 (1993); G. Kresse and J. Furthmuller, *Phys. Rev. B* **54**, 11169 (1996).
¹⁰ A. I. Liechtenstein et al., *Phys. Rev. B* **52**, R5467 (1995).
¹¹ S. L. Dudarev et al., *Phys. Rev. B* **57**, 1505 (1998).
¹² J. B. Neaton et al., *Phys. Rev. B* **71**, 014113 (2005).
¹³ P. Baettig et al., *J. Am. Chem. Soc.* **129**, 9854 (2007).
¹⁴ P. E. Blochl, *Phys. Rev. B* **50**, 17953 (1994).
¹⁵ G. Kresse and D. Joubert, *Phys. Rev. B* **59**, 1758 (1999).
¹⁶ H. J. Monkhorst and J. D. Pack, *Phys. Rev. B* **13**, 5188 (1976).
¹⁷ R. D. King-Smith and D. Vanderbilt, *Phys. Rev. B* **47**, 1651 (1993).
¹⁸ H. T. Stokes et al., *Acta Cryst. B* **B58**, 934 (2002).
¹⁹ C. Michel et al., *Solid State Commun.* **7**, 701 (1969).
²⁰ A. A. Belik et al., *J. Am. Chem. Soc.* **128**, 706 (2006); A. A. Belik et al., *J. Am. Chem. Soc.* **129**, 971 (2007).
²¹ L. Pálová, P. Chandra and K.M. Rabe, in preparation.
²² C. Ederer and N. A. Spaldin, *Phys. Rev. B* **71**, 060401(R) (2005).